Dependence of Basal Fluid Pressure on Fluidization Characteristics in Granular Mass Flow

Yasuhiko Okada[1)] and Hirotaka Ochiai[2)]
1) Department of Soil and Water Conservation, Incorporated Administrative Agency Forestry and Forest Products Research Institute, 1 Matsunosato, Tsukuba, Ibaraki 305-8687, Japan (okada10@ffpri.affrc.go.jp)
2) Department of Soil and Water Conservation, Incorporated Administrative Agency Forestry and Forest Products Research Institute, 1 Matsunosato, Tsukuba, Ibaraki 305-8687, Japan (ochi@ffpri.affrc.go.jp)

Abstract

In order to clarify the fluidization characteristics in the assembly of granular mass, the quasi-real scale flume (totally 13 m long) tests are conducted in which the focus is placed on how much pore-pressure is generated and how long the granular mass travels. Since the generation of excessive pore-pressure is considered one of the most important factors for the rapid motion and long travel distance, the detailed examination of the changes in the pore-pressure must be conducted for the granular mass flow. In this study, the influence of the width of the channel on the fluidization behaviour has been examined. The pumice gravel, and the mixture of pumice gravel and volcanic ash are used for the experiments. No excessive pressure head was observed in the pumice gravel sample. On the other hand, the pressure head at least 1.8 times as much as the normal flow depth of the granular mass at peaks have been measured in the mixture of pumice gravel and volcanic ash, indicative that excessive pressure head must have been generated in the assembly. Both of the samples have traveled shorter in the narrow channel than in the wide one, the mixed sample rather could go through the stricture smoothly. This could be such that the less frictional resistance has been mobilized due to the excessive pore-pressure generation and it has allowed the quasi-liquid subset of granular mass to pass through the stricture in the mixed sample.

Keywords: excessive pore-pressure, granular mass flow, travel distance, fine particle, flow depth

Introduction

The heavy rainfall and earthquakes are the major inducements to landslides, in which the flow-type one is considered one of the most dangerous from the socioeconomic viewpoints because of its high velocity and long run-out distance. The flow-type landslides seem to take place mainly because the rise in the subsurface water table resulted in the break of geomechanical balance among the channel sediments, the slope failure associated the saturated downslope torrent deposits with the liquefied motion, and the failed mass clashed to the check dams suffering from the liquefaction. In the study of the fluidization mechanisms in the flow-type landslides, Shreve (1966, 1968) proposed "the air-layer lubrication model," and Sassa (1996) and Sassa et al. (1996) introduced "the sliding-surface liquefaction model" by keeping eyes on the phenomenon happening in the shear zone. In the air-layer lubrication model, the long run-out distance is explained like the failed landslide mass entrapped the large volume of air at its base and so the coefficient of friction against the slope surface is small due to the high air pressure. The sliding-surface liquefaction is different from the liquefaction phenomena that generates whole in the horizontal sand layer mainly by earthquakes (Casagrande 1971, Castro and Poulos 1977).

It is the localized liquefaction phenomena within the sliding zone, where grain crushing and comminution dominate. Given the undrained conditions, the tendency of volume shrinkage due to grain crushing and comminution generates the pore-pressure, resulting in the reduction of shear resistance. Also Okada et al. (2004) pointed out that the crushed and comminuted grains decreased the bulk permeability within the shear zone, and this less-permeable shear zone prevented the generated excess pore-pressure from dissipation, suffering from the fluidized long travel motion.

On the contrary, Bagnold (1954) proposed "the grain flow model" focusing the phenomenon that is taking place in the granular flow layer. In his model, the grains were well disperse due to the grain collisions and resulted in the small frictional coefficient in the mass flows. Savage (1984) introduced a dimensionless number (Savage number: N_{SAV}) that estimates the ratio of grain-collision stresses to gravitational stresses in steady, gravity-driven flows. Savage and Hutter (1989) estimated that grain-collision stresses become important when N_{SAV} is larger than 0.1. Otherwise, gravity dominates stresses at grain contacts. Iverson and Denlinger (2001) calculated the N_{SAV} for the granular mass flow and proposed that the prevalence of small values of

pp. 437–446

Photo. 1. The model flume for the granular mass flow experiments.

N_{SAV} lead to the hypothesis that Coulomb friction commonly generates most shear resistance in granular mass flow. Iverson and Vallance (2001) mentioned the strong influence of the flow depth, grain concentration, and pore-fluid pressure, especially excessive pore-pressure on the mobilization of granular mass flow.

In light of these mentioned above, the authors conducted the quasi-real scale flume tests on pumice gravel sample, and the mixture of pumice and volcanic ash, in order to empirically prove the fluidization characteristics in the assembly of granular medium, in which the normal flow depths and the changes in basal fluid pressure were carefully monitored as the key elements.

Experimental procedures

Model flume and data acquisition system

The view of employed model flume is shown in Photo. 1 and schematic illustration and the location of the sensors is shown in Fig. 1. The model flume consists of two parts: the upper one is capable for changing the gradient from 10 through 45 degrees, and the other lower one is horizontal but possible for changing the width of the flume. The inclined segment is 5 m long, 0.6 m wide, and 1 m high. The horizontal portion is 8 m long, 1 m high, and the width can be set at 0.3, 0.6, and 1.2 m for the respective experiments (see vertical view illustration in Fig. 1). The one side of the flume is covered by the reinforced glass, therefore it allows to film the movement of the granular mass. In order to splash the assembly of granular materials, the 0.6 m^3 sample was set in the upper end of the slope portion closed by the water-proof gate. The casement gate was controlled by the electric signal at the start of the experiments.

The changes in basal fluid pressure and the flow depth of the produced granular mass flow are the main subjects in a series of our experiments, and so the pore-pressure transducers were set at the base of the flume and the laser displacement transducers were adjusted to monitor the normal flow depth just on the pore-pressure transducers. These data was stored in the PC at 100 Hz. Also the soil movements were monitored by four high-speed cameras and six usual digital video cameras. The high-speed cameras were completely synchronized with each other and they recorded 125 films per second respectively. Around the model flume, four time-code indicators were set to show the elapsed time, the digital video cameras and at least one high-speed camera were placed at which they could film the time-code indicators. Because of this, the data of pore-pressure and flow depth, and filmed images were to be synchronized in the analysis. In addition, the time-code was generated from the commencement of measurement, hence the time "zero" did not mean the outbreak of the casement gate.

Sample and test conditions

Two samples were employed. One (hereafter called sample 1) is the pumice gravel (bora) and the other (sample 2) is the mixture of pumice gravel and volcanic ash, those had been excavated from the Sakurajima Volcano, in Kagoshima prefecture, Japan. Because the bora contained grains with wide variety in size, the particles larger than 50 mm were eliminated by sieving in consideration of the size of model flume. The density of particles was 2,430 kg/m^3 for bora sample and 2,790 kg/m^3 for volcanic ash, respectively. In order to make the specified specimens, the bora was further screened by 20-mm-sieve and 10-mm-sieve. The sample 1

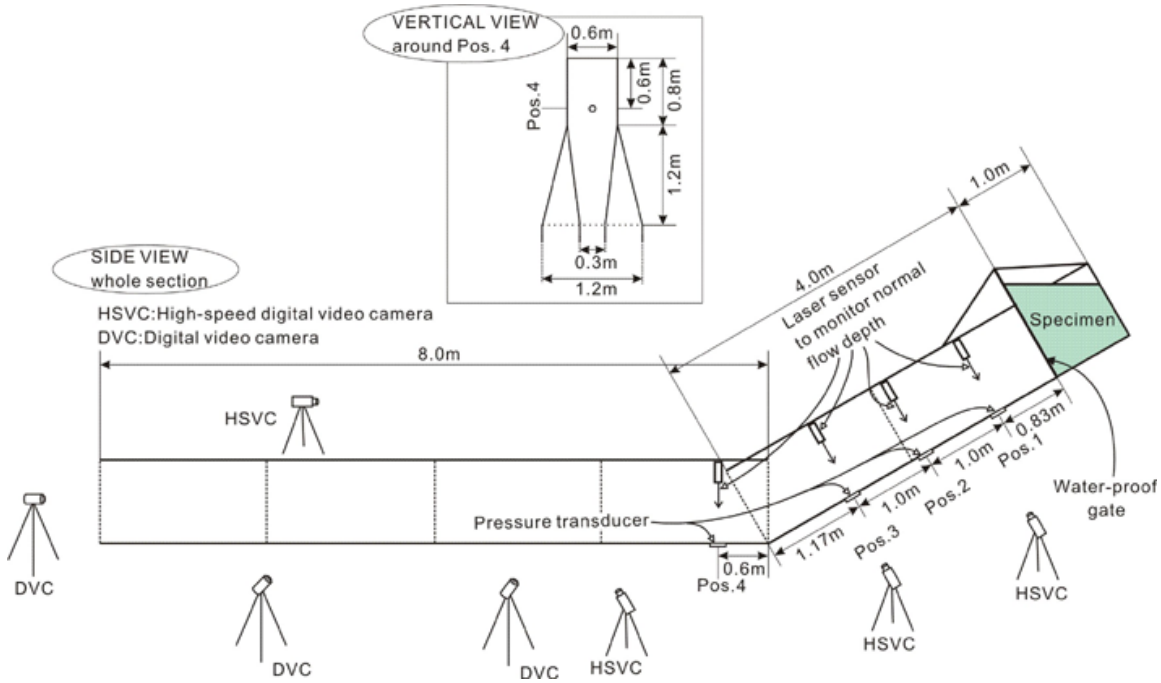

Fig. 1. he schematic illustration of model flume and the arrangement of measurement transducers.

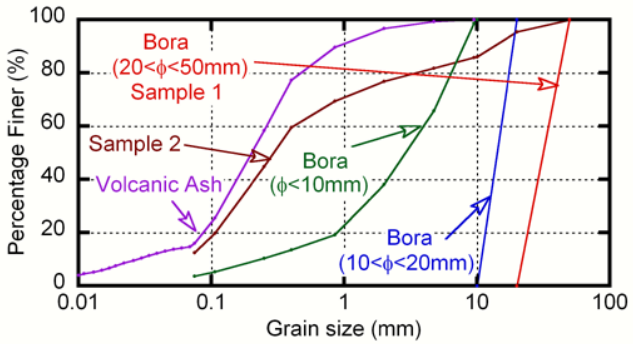

Fig. 2. The grain size distributions curves of the employed materials.

consisted of bora of 20 mm $\leq \phi <$ 50 mm. The sample 2 was mixed with the bora (20 mm $\leq \phi <$ 50 mm, 10 mm $\leq \phi <$ 20 mm, $\phi <$ 10 mm) and volcanic ash at one-two-two-five ratio in volume when they were pluviated in the 0.04 m^3 bucket. After the sample were formed at the upper end of the slope portion set at 10 degrees, water was slowly percolated from the bottom for more than two hours to make specimen saturated. After saturation, the slope portion was changed to 30 degrees before the tests. The grain size distribution curves are shown in Fig. 2 and Table 1 summarizes the test conditions.

Test results and discussion

Changes in basal fluid pressure and normal flow depth in slope-section

The dynamic fluctuations of the basal fluid pressure and the normal flow depth were monitored in the slope-section (Pos. 1, 2, and 3) and at the position located around the connection between slope- and horizontal-section (Pos. 4). Pos. 4 is also located at the mouth of width-changed point of the horizontal section (See Fig. 1). Fig. 3 shows the obtained changes in basal fluid pressure and normal flow depth of Test 1-1 on the slope-section. The values of normal flow depth started to increase in downslope sequence at 11.08 sec (pos. 1 in Fig. 3(a)), 11.72 sec (pos. 2 in Fig. 3(b)), and 11.85 sec (pos. 3 in Fig. 3(c)). Within one second they exhibited the peak at 11.90 sec (pos. 1), 12.23 sec (pos. 2), and 12.50 sec (pos. 3), and then they decreased to almost zero until 16.0 sec for all slope section. At position 1, the normal flow depth once showed maximal before the

Table 1. Test identification numbers and conditions.

Test number	Material	Width of horizontal section (m)	Initial void ratio, e_0
Test 1-1	Sample 1	0.30	4.8
Test 1-2	Sample 1	1.2	4.6
Test 2-1	Sample 2	0.30	0.92
Test 2-2	Sample 2	1.2	0.95

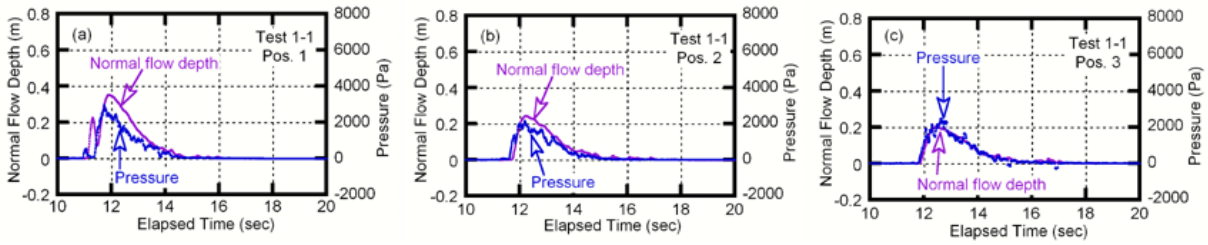

Fig. 3. The changes in basal fluid pressure and normal flow depth of Test 1-1 in slope section (Pos. 1, 2, and 3).

peak at about 11.3 sec. This was likely attributable to the firstly-spilt materials before the casement gate was completely open. The downslope velocity between position 2 and position 3 was larger than 5.5 m/sec (25.2 km/hour), it was 7.69 m/sec at the front of the granular assembly and it was 5.88 m/sec when normal flow depth was at peak. Because the position 1 was located closer to the water-proof casement gate, the peak value of normal flow depth reached 0.35 m, larger than those at position 2 and position 3. However, the changing trend of normal flow depth after the peak was quite similar for all positions. It means that, after the gate-open, the whole portion of pumice gravel sample traveled downslope in one spurt from upper slope-section to lower slope-section.

Focusing on the dynamic changes in basal fluid pressure, it could be noted that the basal fluid pressure were strongly influenced by the normal flow depth such that the values of basal fluid pressure were in general increased when the values of normal flow depth were increased and vice versa. The values of basal fluid pressure started to increase from 11.31 sec (pos. 1 in Fig. 3(a)), 11.60 sec (pos. 2 in Fig. 3(b)), and 11.77 sec (pos. 3 in Fig. 3(c)) respectively. They showed the peaks of 2,961 Pa at 11.73 sec (pos. 1 in Fig. 3(a)), 2,151 Pa at 12.20 sec (pos. 2 in Fig. 3(b)), and 2,482 Pa at 12.64 sec (pos. 3 in Fig. 3(c)), and they remained almost zero from 15.5 sec in all positions.

Whereas, the changes in basal fluid pressure and normal flow depth of Test 2-1 on the slope-section are shown in Fig. 4. Also the normal flow depth started to increase its values in downslope sequence at 12.95 sec (pos. 1 in Fig. 4(a)), 13.19 sec (pos. 2 in Fig. 4(b)), and 13.38 sec (pos. 3 in Fig. 4(c)) and it reached peak at 13.32 sec (pos. 1), 13.75sec(pos. 2), and 13.99 sec (pos. 3). After showing peak, the normal flow depth decreased its values in similar way for all slope-section, however it did not returned to zero, indicating that there were some materials slowly moving along the slope. The downslope velocity between position 2 and position 3 was larger than 4.0 m/sec (18.0 km/hour), it was 5.26 m/sec at the front of the granular assembly and it was 4.17 m/sec when normal flow depth was at peak. Although some portions of materials were still moving slowly along the slope-section, the majority traveled downslope with high speed of 18.0 km/hour.

The attention being paid to the changes in pore-pressure, the basal fluid pressure in Test 2-1 also seemed to be controlled by the normal flow depth. Although the increasing and decreasing rates of the values were rather different, the values of basal fluid pressure increased/decreased when the values of normal flow depth increased/decreased. It should be mentioned that the quite large values of basal fluid pressure was observed at position 1 around 13.11 sec. This was probably because position 1 was too close to the casement gate, so the subset of materials flied to position 1 in prevalence of vertical motion resulting in the clash. As for positions 2 and 3, the assembly of granular materials reached there without the fall from the casement gate. The values of basal fluid pressure increased from 12.90 sec (pos. 1 in Fig. 4(a)), 12.99 sec (pos. 2 in Fig. 4(b)), and 13.22 sec (pos. 3 in Fig. 4(c)). They showed peaks of 6,761 Pa at 13.10 sec (pos. 1 in Fig. 4(a)), 3,146 Pa

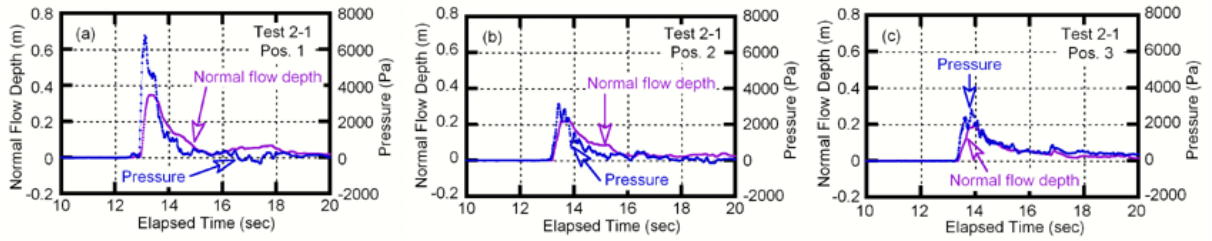

Fig. 4. The changes in basal fluid pressure and normal flow depth of Test 2-1 in slope section (Pos. 1, 2, and 3)

at 13.45 sec (pos. 2 in Fig. 4(b)), and 2,818 Pa at 13.86 sec (pos. 3 in Fig. 4(c)), hence the values at peaks were decreased in the downslope sequence. The values of basal fluid pressure remained almost zero from about 19 sec at positions 1 and 2, whereas at position 3, they did not returned to zero associated with the slow movement of the assembly of granular materials.

Run-out behaviour at around width-changed point

The changes in basal fluid pressure and normal flow depth at around the width-changed point (position 4) are shown in Fig. 5. The results of Tests 1-1, 1-2, 2-1, and 2-2 are Fig. 5(a), (b), (c), and (d), respectively. Test 1-1 increased the values of normal flow depth from 11.98 sec to 13.96 sec, after that the normal flow depth were constant at 0.45 m when the materials deposited (Fig. 5(a)). Because the horizontal flume-section for Test 1-1 narrows its width to 0.3 m, the traveled materials along the slope-section rushed to the stricture resulting in the jam, which yielded the high normal depth at position 4. The basal fluid pressure simultaneously increased its values with normal flow depth, it reached not more than 3,667 Pa at 13.96 sec, after that it decreased gradually. As for Test 1-2 (Fig. 5 (b)), the normal flow depth started to increase at 13.17 sec to reach peak of 0.19 m at 13.96 sec prior to the reduction to 0.066 m until 17.53 sec. After 17.53 sec, it reincreased to 0.082 m at 34.98 sec, and then reduced its values slowly. The first sharp peak was likely attributable to the effect of the change in the flume gradient (position 4 was located around the connection between the slope- and horizontal-section). The conspicuous difference from Test 1-1 was that the normal flow depth was slowly changing even until 100 sec, indicating the very slow movement of the material took place. Since Test 1-2 was conducted for the horizontal-section of 1.2 m width, no jam as being caused in Test 1-1 was formed so the assembly of granular materials moved slowly forward with the inertia force. The changes in basal fluid pressure were almost the same as the one of normal flow depth. The difference was that the values of basal fluid pressure changed dynamically between 13.30 sec and 16.26 sec, when the front surge of materials passed through position 4. This was likely because the traveling materials could be rather jumping and falling due to the effect of the gradient change of the flume. As for Test 2-1 (Fig. 5(c)), the values of normal flow depth started to increase from 13.56 sec and decrease from 13.96 sec. After that it reincreased from 15.95 sec, then it was almost constant from 23.00 sec. The basal fluid pressure almost traced the normal flow depth until 16.34 sec, after that the basal fluid pressure greatly increased to reach peak of 2,912 Pa at 42.91 sec. After showing peak, also the basal fluid pressure was almost constant. The changes in basal fluid pressure and the normal flow depth in Test 2-2 (Fig. 5(d)) were quite similar to those in Test 2-1. Until 16.34 sec, the changes in both parameters were in good harmony with each other, after 22.69 sec the basal fluid pressure decreased and the normal flow depth increased very slowly. The peak value of basal fluid pressure after 22.69 sec was 1,358 Pa at 34.58 sec, when the normal flow depth was at 0.089 m. Because Test 2-2 had wider flume (1.2 m wide), the normal flow depth was smaller than that in Test 2-1 (0.3 m wide).

Generation of Excessive pore-pressure

As generally noted, the generation of excessive pore-pressure is likely the most important factors for the rapid motion and long travel distance of the granular mass flow. Since the soil particles are somewhat liable to float in the pore fluid due to the high fluid pressure, the effective normal stress mobilizing between soil particles reduced and it lead to the loss of shear resistance. In this case, the high fluid pressure is generated both by the suspension of finer materials that apparently increase the mass density of fluid and by the undrained deformation within the assembly of soil mass. Iverson (1997) pointed out, if a particle can remain suspended as a result of viscous resistance of water, the particles may act as part of fluid and these particles are with diameters less than about 0.05 mm (silt and clay particles). In our experiments, the higher basal fluid pressure

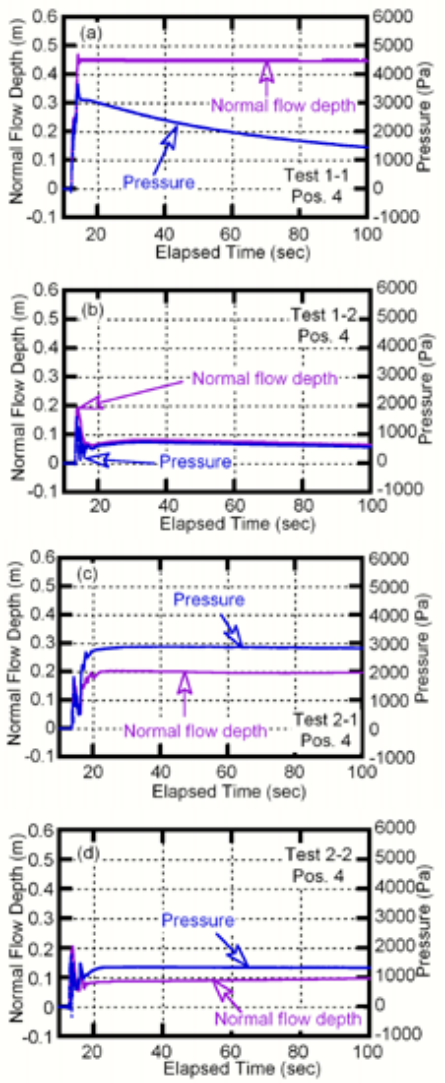

Fig. 5. The relationship between basal fluid pressure and normal flow depth of Test 1-1, 1-2, 2-1, and 2-2 at the mouth of width-changed point (Pos. 4).

was observed in the mixed sample of pumice gravel and volcanic ash (sample 2. See Fig. 3 and Fig. 4). Since this sample contains finer particles (less than 0.075 mm) about 12 % by weight, the effect of suspension might not be neglected in the evaluation of higher fluid pressure observed in the Test 2-1 and 2-2. If the pore fluid does not contain any finer particles suspended, its mass density is 1,000 kg/m^3. However, the apparent mass density of fluid with suspended particles must have larger density and Iverson (1997) explained the mass density of flow fluid ρ_f can be calculated by the following equation and illustrated that the density of sand-gravel-loam mix sample varied between 1,120 through 1,200 kg/m^3.

$$\rho_f = \rho_s \nu_{fines} + \rho_w (1 - \nu_{fines})$$

where ρ_{fines} is the mass density of fine particles, and ρ_w is the mass density of pure water. If all silt- and clay-size particles were suspended, mass density of fluid in sample 2 could have been 1,191 kg/m^3, and this value is within the range pointed out by Iverson (1997). Hence the pressure head at the base of the flume generated in Test 2-1 and 2-2 could be estimated as the division of basal fluid pressure by the mass density of fluid (1,191 kg/m^3) and gravitational acceleration. Although the water table and the normal flow depth of the granular mass flow would be different, the difference between estimated pressure head and the normal flow depth should be one parameter that designates the excessive pressure head. Figs. 6 (a) through (e) show the changes in those estimated excessive pressure head at positions 1, 2, 3, and 4 in Test 2-1 and position 4 in Test 2-2. It is obvious from these figures, the positive excessive pressure head was observed at all positions. The peak values of positive excessive pressure head were 0.40 m at 13.02 sec (Fig. 6(a)), 0.12 m at 13.41 sec (Fig. 6(b)), 0.11

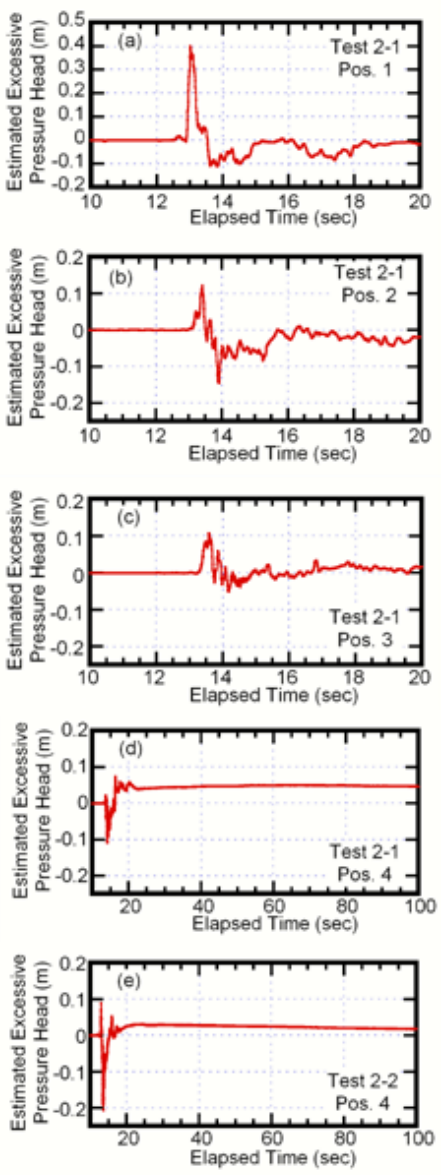

Fig. 6. The changes in estimated excessive pressure head in Test 2-1 (Pos. 1, 2, 3, and 4) and Test 2-2 (Pos. 4).

m at 13.59 sec (Fig. 6(c)), 0.073 m at 16.39 sec (Fig. 6(d)), and 0.088 m at 12.98 sec (Fig. 6(e)). Hence, the excessive pressure of not less than 0.1 m was generated along the slope-section in the front surge of the granular flow. The excessive pressure head at position 4 in Test 2-1 and Test 2-2 (Figs 6(d) and (e)) remained positive from about 16 sec even until 100 sec, indicative that the generated excessive pressure head was prevented from dissipating when the granular mass almost stopped and deposited. The ratios of peak excessive pressure head to the normal flow depth at the same elapsed times at all positions are shown in Fig. 7. The position 1 located close to the casement gate showed the quite large value, however, it must be due to the clash of the falling soils onto the flume base. Except for the position 1, the ratios ranged between 1.8 through 4.1 and this result established the fact that the excessive pore-pressure must be generated in the assembly of granular soils during the flow motion in sample 2. When the subset of granular mass traveled along the flume, the flow depth was at most 0.3 m or so and the upper surface of the materials was in contact with the air. However, the pressure head in the front surge of the assembly of granular mass allowed the pressure head to exceed the normal flow depth, indicative that the undrained conditions which were usually given in the geotechnical soil tests such as the triaxial compression and the ring-shear tests were likely maintained. The study of the granular mass flows like debris flows in rheological viewpoints often precludes the dynamic changes in pore water pressure (Iverson, 1997), however it is necessary that the existence of excessive pressure head at least in the front surge

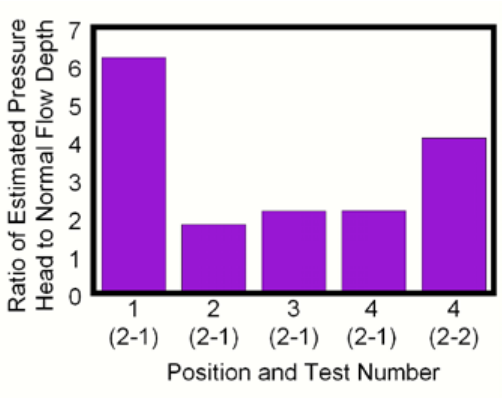

Fig. 7. Ratio of estimated pressure head to normal flow depth at peaks of estimated excessive pressure head.

of granular flow should be taken notice of in the evaluation of flowing mechanisms of granular materials.

Equivalent Coefficient of friction

The side views of the deposited granular materials are shown in Figs. 8(a), (b), (c), and (d) for Test 1-1, 1-2, 2-1, and 2-2 respectively. Also the positions of gravity centre when deposited are mentioned in these figures. The widths of the horizontal-section are in two values, 0.3 m and 1.2 m, however, these figures neglect this difference. Actually, only the small differences in the posture of deposits in the cross sectional direction were observed. As Fig. 8(a) shows, the sample 1 (Test 1-1) mostly deposited around the connecting point between slope- and horizontal-section. As was discussed in the previous sub-section, this was due to the narrowing change of the width of flume, resulting in the clogging around there. On the other hand, the sample 2 (Test 2-1) deposited rather homogeneously along the horizontal-section and it reached almost the end of the flume, in which the clogging unlikely occurred. As for Test 1-2 and 2-2 which were conducted with the wide flume, both samples deposited rather even. It should be mentioned here that the sample 2 in Test 2-2 passed through the end of the flume and the amount of 0.025 m^3 were deposited outside.

The calculated equivalent coefficients of friction were in the orders of test numbers, such as 17.2 degrees for Test 1-1, 16.6 degrees for Test 1-2, 14.9 degrees for Test 2-1, and 14.6 degrees for Test 2-2 (see Fig 8). Here, note that the effect of the materials that passed through the flume was neglected in the calculation for Test 2-2. The equivalent coefficients of friction of the sample 2 were smaller than those of sample 1. This fact must depend on the pore-pressure behaviour that was discussed in the previous sub-section, in which excessive pressure head was observed only in the sample 2 to reduce the effective normal stress acting on the particles leading to the loss of shear resistance. Given the attention being paid to the flume conditions, for both two samples, the tests with wide flume (Test 1-2 and 2-2) produced the smaller equivalent coefficients of friction than those with narrow flume (Test 1-1 and 2-1). This was likely because the clogging took place at the stricture, and more frictional collisions against the side-walls occurred resulting in the larger resistance for Tests 1-1 and 2-1 with narrow flume. On the other hand, the samples went through smoothly around the connecting point and less collisions against side-walls and resulting grains' contacts occurred for Tests 1-2 and 2-2 with wide flume.

Conclusions

The quasi-real scale flume tests were conducted in order to reveal the pore-pressure behaviour and run-out characteristics of pumice gravel sample and the mixture of pumice and volcanic ash. The experiments drew the followings:

1. Excessive pressure head at least 1.8 times of the normal flow depth was observed in the front surge of the granular mass flow along the slope-section for the tests with mixture of pumice gravel and volcanic ash. Whereas, no excessive pressure head was observed in the pumice gravel sample. The mixture of pumice gravel and volcanic ash produced smaller equivalent coefficients of friction than those of the pumice gravel sample. This could explain that the generation of excessive pore-pressure head affected the long run-out distance of granular mass flows;

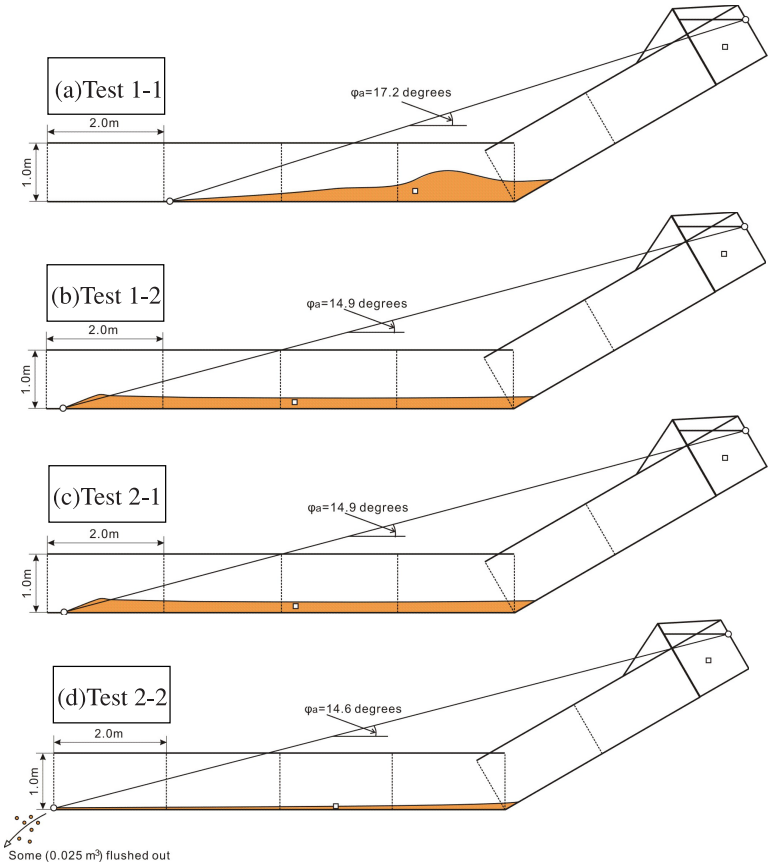

Fig. 8. The side view of the depositions of granular mass. The equivalent friction angle and the positions of gravity centers are also shown.

2. In the test on the pumice gravel sample with narrow flume, the clogging took place around the stricture, the most material deposited around the stricture without excessive pressure head and they did not travel long distance. On the other hand the mixture sample did not make the heap around the stricture, the assembly of granular materials went through smoothly with excessive pressure head 2.1 times as much as the normal flow depth. Hence, the stricture was not strong obstacles for the quasi-liquid subset of materials; and
3. Both of the samples run-out longer along the wide flume than the narrow flume. This was likely because, in the tests with wide flume, no clogging took place where the width of the flume changed and less frictional collisions against side-walls and resulting grains' contacts occurred.

References

Bagnold, R.A. (1954) Experiments on a gravity-free dispersion of large solid spheres in a Newtonian fluid under shear. Proceedings of the Royal Society of London. Mathematical and physical sciences. **225A**, pp. 49–63.

Casagrande, A. (1971) On liquefaction phenomenon. Géotechnique. **21**(3), pp. 197–202.

Castro, G., and Poulos, S.J. (1977) Factors affecting liquefaction and cyclic mobility. Journal of Geotechnical Engineering Division, ASCE. **103**(GT6), pp. 501–516.

Iverson, R.M. (1997) The physics of debris flow. Reviews of geophysics. 35, pp. 245–296.

Iverson, R.M., and Denlinger, R.P. (2001) Flow of variably fluidized granular masses across three-dimensional terrain 1. Coulmob mixture theory. Journal of Geophysical Research. **106**(B1), pp. 537–552.

Iverson, R.M. and Vallance, J.W. (2001) New views of granular mass flows. Geology. **29**(2), pp. 115–118.

Okada, Y., Sassa, K., and Fukuoka, H. (2004) Excess pore pressure and grain crushing of sands by means of undrained and naturally drained ring-shear tests. Engineering Geology. **75**(3), pp. 325–343.

Sassa, K. (1996) Prediction of earthquake induced landslides, Special Lecture of 7th International Symposium on Landslides, "Landslides," Trondheim, 17–21 June, Balkema, **1**, pp. 115–132.

Sassa, K., Fukuoka, H., Scarascia-Mugnozza, G., and Evans, S. (1996) Earthquake-induced-landslides: Distribution, motion and mechanisms. Soils and Foundations. Special Issue for the great Hanshin Earthquake Disasters, pp. 53–64.

Savage, S.B. (1984) The mechanisms of rapid granular flows. Advanced Applied Mechanics. **24**, pp. 289–366.

Savage, S.B., and Hutter, K. (1989) The motion of a finite mass of granular material down a rough incline. Journal of Fluid Mechanics. **199**, pp. 177–215.

Shreve, R.L. (1966) Sherman landslide, Alaska. Science. **154**, pp. 1639–1643.

Shreve, R.L. (1968) Leakage and fluidization in air-layer lubricated avalanches. Geological Society of America Bulletin. **79**, pp. 653–658.